 doi:10.20944/preprints202205.0355.v1

Article

Modeling of Energy and Exergy Efficiencies in High Vacuum Flat Plate Photovoltaic Thermal (PV-T) Collectors

Daniela De Luca[1,2,*], Antonio Caldarelli[2,3], Eliana Gaudino[2,3], Emiliano Di Gennaro[1,2], Marilena Musto[2,3] and Roberto Russo[2]

[1] Physics Department, University of Napoli "Federico II", Complesso Universitario di Monte Sant'Angelo, Via Cinthia, 21, 80126 Napoli, Italy
[2] Institute of Applied Sciences and Intelligent Systems, National Research Council of Italy, via Pietro Castellino 111 80131 Napoli, Italy
[3] Industrial Engineering Department, University of Napoli "Federico II", Piazzale Vincenzo Tecchio, 80, 80125 Napoli, Italy
*Corresponding author: daniela.deluca@unina.it

Abstract: This work deals with the performance evaluation of novel flat photovoltaic-thermal (PV-T) modules under vacuum. Through a 1D (dimensional) steady-state-energy-balance numerical model developed in MATLAB, two different layouts are studied: the first consisting of a photovoltaic (PV) cell installed just below the glass encapsulating the flat panel, and the second where the PV cell is placed on the selective solar absorber (SSA). In both cases the thermal and electrical efficiencies have been evaluated at different SSA operating temperatures, in the range of 323 K to 423 K. The analysis has been conducted at different energy bandgap (E_{bg}) of the PV cell and assuming a variable transmittance or emittance of the PV cell, depending on the design. The two systems efficiency comparison has been carried out at the same operating temperature. Overall, this work highlights the importance of high vacuum insulation, which guarantees the reduction of convective thermal losses, and shows that the maximum energy is produced for PV cells with E_{bg} ≈1.5-1.7 eV, depending on layout and operating temperature, by including the thermal output in the PV-T optimization. The energy and exergy efficiencies obtainable using the proposed PV-T systems are considerably improved compared to the results previously reported in the literature.

Keywords: solar energy; photovoltaic-thermal; electrical efficiency; thermal efficiency; exergetic efficiency; high-vacuum; evacuated flat plate

1. Introduction

While green electricity is the indisputable key energy carrier for a climate neutral future in energy supply, nearly half of the energy consumed globally is finally used as heat, ranging from low temperature domestic hot water and space heating, up to medium and high-grade industrial-scale applications. In this context, solar-thermal (ST) and photovoltaic (PV) panels represent key solutions to the mitigation of the climate crisis and the production of decarbonized electricity and heating. Despite the photovoltaic solar energy capacity worldwide has grown, commercial PV panels convert only approximately the 25% of the absorbed solar energy into electricity (Green et al., 2020), dissipating the rest of the absorbed energy as waste heat (Teo et al., 2012) that causes an increase of temperature in the PV cell and leads to a decrease in the PV efficiency (Dubey et al., 2013). Distributed multi-energy systems can offer advantages in clean energy supply in terms of overall performance and enhanced flexibility. In the case of hybrid solar/PV-Thermal (PV-T) technologies, it allows to maximize the energy yield per unit of available space and to deliver it at lower cost, by generating both heat and electricity (Herrando et al., 2014). Thermal and electrical energy outputs depend on many factors: irradiance, ambient temperature, wind speed, circulating fluid temperature, flowrate, etc. (de Keizer et al., 2016). However, solar electricity and solar heat combined can serve the heating and

 doi:10.20944/preprints202205.0355.v1

cooling (H&C) applications, while also powering new industrial processes to produce new green energy carriers, like hydrogen or processes for Carbon Capture and Utilization (CCU), and any other future application which will require both electricity and heat vectors to operate.

PV-T technologies have been studied since the 1970s, including variation in designs, working fluids and other performance-influencing factors (Chow, 2010; Zondag, 2008). Nevertheless, research continues with the aim of obtaining a design offering a combination of high thermal and electrical efficiencies, reliability, and low cost. The most common PV-T collector type has a flat-plate design, although a recent work (Baljit et al., 2017) modeled a dual-fluid concentrating PV-T solar collector showing that the total equivalent efficiencies ranged from approximately 30 to 60% in the case of single fluid condition and reached approximately the 90% in the case of the dual fluids. Indeed, the dual fluids operation mode reduced the solar cells temperature and hence increased the electrical output. However, those systems are linked with high costs and reduced performance in areas with high proportion of diffuse solar irradiance (Khlief et al., 2021). In the flat-plate layout, the performance of PV-T systems has been estimated by different numerical models using steady-state (Sahlaoui et al., 2021; Salameh et al., 2021) or transient conditions (Maleki et al., 2021). However, all the PV-T systems developed and designed so far have been driven in the perspective of maximizing the production of electricity, conveying only the residual energy towards thermal conversion. Indeed, normally the thermal energy generated by such collectors would be useful for domestic use or low-temperature industrial processes (Herrando et al., 2021; Shaari et al., 2014): experimental analysis on existing PV-T systems have shown that users can satisfy their needs for low temperature heat (e.g., water at 30-40 °C) during summer, but the high thermal losses forbid to generate usable heat during winter or at temperatures higher than 50 °C even during summer.

The recent introduction on the market of evacuated flat plate (EFP) collectors (Buonomano et al., 2016) have opened new possibilities in the development of high efficiency systems that include a standard PV-T collector in a flat and evacuated layout: Mellor et al. (Mellor et al., 2018) demonstrate the great energetic advantage obtained by using evacuated flat PV-T collectors in combination with low-emissive coatings. Indeed, compared to present commercial TPVs, a system that employs an evacuated glazing cavity combined with a low emissive coating (ε=0.15) is expected to have double the thermal efficiency, and to provide 1.5 and 2 times the revenue or carbon savings of PV modules and solar thermal collectors, respectively. However, the proposed configuration presents two disadvantages: on one hand the metallic sheet reflects the photons with energy lower than the silicon energy bandgap (E_{bg}=1.1 eV), losing about the 19% of the total solar energy; on the other hand, the PV cell is laminated on the metal foil using polymeric/organic foils, a technique not suitable for high vacuum. Nevertheless, the idea of a PV cell under vacuum paves the way for improving the performance of PV-T systems by increasing the production of thermal energy at high operating temperatures. Therefore, we propose a *new generation of hybrid solar collectors* that allow us to maximize solar energy conversion and meet the demand for medium temperature heat while producing electricity for a wide range of multi-energy systems. Consequently, we reconsider the definition of the optimal energy bandgap of a single PV cell taking into account the production of thermal energy along with the Shockley-Queisser (SQ) limit (Queisser, 2009; Rühle, 2016). In this work we present and compare two under-vacuum PV-T layouts: the first one where the PV cell is positioned just below the glass encapsulating the flat panel, acting as a spectral splitter (Huang and Markides, 2021) (layout **A**), and the second one where the PV cell is placed on the absorber, which is mainly developed as a selective solar absorber (SSA, layout B). It is equipped with a high thermal conductive and low emissive substrate, such as aluminum, which draws the heat away and allows the vessel to remain at ambient temperature. Fig. 1 shows the simplified cross-section of both layouts (Fig. 1 a, b) and the correspondent solar spectrum utilization (Fig. 1 c, d).

Preprints (www.preprints.org) | NOT PEER-REVIEWED | Posted: 26 May 2022 doi:10.20944/preprints202205.0355.v1

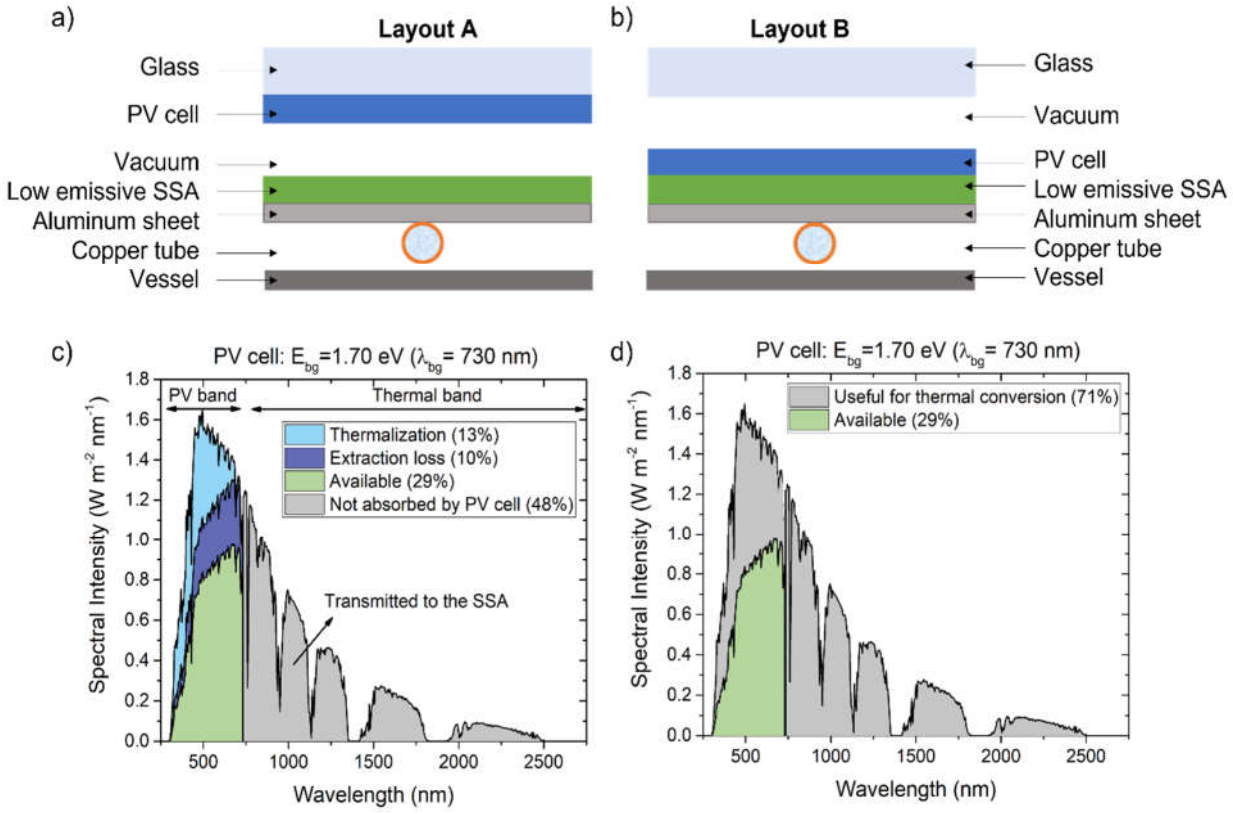

Figure 1. Cross-section schematic of the two evacuated PV-T collectors' layouts: (a) layout **A** (PV cell below the glass encapsulating the flat panel) and (b) layout **B** (PV cell above the absorber). Solar irradiation spectrum (ASTMG173) utilization of a semi-transparent solar cell with λ_{bg}=730 nm, which defines a PV band ($\lambda<\lambda_{bg}$) and a thermal band ($\lambda>\lambda_{bg}$). The integration of the PV cell into the glass (c) allows to transfer only the 48% of the solar radiation to the SSA for thermal energy conversion, while the integration of the PV cell into the SSA (d) allows the entire portion of the solar spectrum not converted into electricity by the PV cell to reach the SSA below (71%).

It is evident how the PV material energy bandgap determines the percentage of photons that are i) absorbed by the PV cell and useful for solar-to-electrical conversion (*available*, green area in Fig. 1), ii) either not absorbed/lost (*thermalization*) or useful for thermal conversion, depending on the layout. The integration of the PV cell into the glass (layout **A**) decouples the thermal and electric output: the PV cell temperature can be controlled by the choice of an appropriate material, which also guarantees a spectral selectivity. However, in this configuration, the fraction of the solar spectrum with $E>E_{bg}$ ($\lambda<\lambda_{bg}$) absorbed by the PV cell and not converted into electricity (blue and light blue areas in Fig. 1 c)) is transformed into heat, and hence wasted. Conversely, if the PV cell is fabricated on the SSA (layout **B**), this excess energy will generate heat which adds to the heat produced by the SSA. Thus, the entire portion of the solar spectrum that is not converted in electricity can be recovered by the SSA below, increasing the fraction of solar radiation available for thermal conversion: in the case of a PV cell with E_{bg} =1.7 eV it reaches the 71% (Fig. 1 d), grey area) versus the 48% of the previous case (Fig. 1 c), grey area).

In both layouts we evaluate the thermal and electrical efficiencies as a function of the PV cell bandgap. We show that, by analyzing the exergy of the system, the optimal bandgap of the PV cell results a function of the PV-T collector layout and of the thermal output temperature.

The manuscript is structured as follows: in Section 2 we show details of our methodology for simulating the performance of high-vacuum PV-Ts in both layouts; in Section 3 we present the main results of the efficiency analysis. Finally, we conclude by summarizing our findings and proposing new perspectives in Section 4.

Preprints (www.preprints.org) | NOT PEER-REVIEWED | Posted: 26 May 2022 doi:10.20944/preprints202205.0355.v1

2. Methodology

The PV-T collectors under study are based on high-vacuum flat plate (HVFP) collectors designed and produced by TVP Solar ("TVP Solar"): they consist of a PV cell and an SSA enclosed between a highly transparent glass cover and a stainless-steel vessel, as schematically shown in Fig. 1. Since the HVFP is 1 m x 2 m wide and only 0.05 m thick, we can safely assume the infinite layers approximation, since the distances between each layer are much smaller than the panel lateral widths. Therefore, the system can be described by the equation of radiative exchange between flat parallel plates in a 1D thermal model that neglects thermal gradient and boundary effects, as already validated a previous work (D'Alessandro et al., 2021). The two different layouts are modeled by using steady state energy balance equations on the three main components of the system: glass cover, PV cell, SSA. In both designs we assumed the Shockley–Queisser limit (Queisser, 2009; Rühle, 2016) to assess the PV cell electrical efficiency, whilst we considered an SSA optimized for non-concentrating applications with high absorptance (α_{SSA}=0.95) and low thermal emittance (ε_{SSA}=0.05) (De Maio et al., 2021a, 2021b) to estimate the thermal efficiency at different SSA operating temperatures (from 323 K to 423 K). The geometric, thermal, and optical characteristics of the modules used in the analysis are reported in Table 1.

Table 1. Geometric, thermal, and optical parameters of each PV-T module.

Layer	Parameter	Variable	Value	Unit	Ref.
Glass	α_g	Absorptance	0.02		
	τ_g	Transmittance	0.94		
	k_g	Thermal conductivity	1.06	W m^{-1} K^{-2}	
	t_g	Thickness	5E-3	m	
PV cell	β	Temperature coefficient	-0.2	%/K	
	t_{PV}	Thickness	1.50E-6	m	
	α_{PV}	Absorptance	0 for E<E_{bg} var. for E>E_{bg}		
	τ_{PV}	Transmittance	1 for E<E_{bg} var. for E>E_{bg}		
	ε_{PV}	Emittance	0.90/var.		
	η_0	Electrical efficiency at T_{amb}	var.		("Infinity PV")
SSA	α_{SSA}	Absorptance	0.95		
	ε_{SSA}	Emittance	0.05		
Others	I	Solar irradiance	1000	W m^{-2}	(Sample and Virtuani, 2009)
	T_{amb}	Ambient Temperature	300	K	
	T_{ves}	Vessel Temperature	300	K	
	T_{NOCT}	Nominal Operating Cell Temperature	323	K	
	ε_{ves}	Vessel emittance	0.15		
	ε_{sub}	Substrate emittance	0.05		
	v_w	Wind velocity	2	m/s	
	$k_{PV\text{-}SSA}$	Equivalent SSA-PV cell thermal conductivity	100	W m^{-1} K^{-1}	

2.1. Layout A: PV cell under the glass

Design. The simplified cross-section of a basic PV-T collector in this layout has been shown in Fig. 1 a): a semi-transparent PV cell is placed on the top layer of the PV-T collector, right under the encapsulating glass. The PV cell acts as a spectral-splitting optical filter (Huang and Markides, 2021): it selectively absorbs part of the incident solar spectrum, which can be partially converted to electricity, and let the remaining fraction of solar radiation pass through and reach the absorber, where thermal energy is produced.

Preprints (www.preprints.org) | NOT PEER-REVIEWED | Posted: 26 May 2022 doi:10.20944/preprints202205.0355.v1

In this setup, the PV-T performance have been studied as a function of the PV cell bandgap, assuming the cell transmittance spectra (τ_{PV}) to be a step function with height equal to 1 for all $\lambda>\lambda_{bg}$ ($E<E_{bg}$), while $\tau_{PV}(\lambda)$ in [0;1] for $E<E_{bg}$: the higher the $\tau_{PV}(\lambda)$, the higher the fraction of the solar spectrum hitting the SSA. Hence, more thermal energy is expected to be produced at the expense of electrical energy.

Thermal model equations. The 1-D thermal model consists of a steady state energy balance equation for each layer of the PV-T module.

The *glass cover energy balance* takes into accounts both convective losses to the external ambient and conductive exchange with the PV cell, in addition to the absorption of the glass itself (α_g):

$$\alpha_g \cdot \int_0^\infty G(\lambda)\, d\lambda + \hbar_w(T_{amb} - T_g) + \frac{k_{PV-g}}{\Delta t}(T_{PV} - T_g) = 0 \quad (1)$$

where $G(\lambda)$ is the spectral distribution of the incident solar radiation, h_w is the heat convection coefficient, $h_w = 4.5 + 2.9\ u_w$ (u_w<5 m/s is the wind speed) (Herrando et al., 2014), $k_{PV\text{-}g}$ the equivalent thermal conductivity of the couple PV cell-glass. Note that $k_{PV\text{-}g} \approx k_g$ as the PV cell thickness is much smaller than that of the glass (≈ μm Vs mm). Hence, $\Delta t \approx t_g$. Finally, the ambient temperature, T_{amb}, is set to 300 K, while T_g and T_{PV} are two of three unknowns of the system. The solar irradiance, $I=\int_0^\infty G(\lambda)d\lambda$ in this study is equal to 1000 W/m^2.

The *PV module energy balance* considers the energy absorbed by the solar cell through the absorption coefficient, defined as $\alpha_{PV}(\lambda, E_{bg}) = 1 - \tau_{PV}(\lambda, E_{bg})$. A fraction of this absorbed radiation is then converted into electrical power; to keep the calculation independent on the choice of the PV material, the converted fraction is calculated using the SQ limit.

Besides the conductive exchange with the glass (already introduced in the previous equation), the PV cell experiences a radiative thermal exchange with the SSA. Hence, the balance equation of the PV module will be:

$$\tau_g \cdot \int_0^\infty G(\lambda)\, \alpha_{PV}(\lambda, E_{bg})d\lambda + \frac{k_{PV-g}}{\Delta t}(T_g - T_{PV}) + \varepsilon_{PV-SSA}(\lambda)\sigma(T_{SSA}^4 - T_{PV}^4) + \eta_{el}\tau_g \int_0^\infty G(\lambda)\, \alpha_{PV}(\lambda, E_{bg})d\lambda = 0 \quad (2)$$

where σ is the Stephan-Boltzmann constant, and $\varepsilon_{PV\text{-}SSA}$ is the equivalent emissivity of the PV cell facing the SSA, calculated as a reduced equation of the radiative heat transfer (Sample and Virtuani, 2009):

$$\varepsilon_{PV-SSA} = \frac{1}{\frac{1}{\varepsilon_{PV}} + \frac{1}{\varepsilon_{SSA}} - 1} \quad (3)$$

The quantity

$$\eta_{el} = \eta_0 \cdot [1 + \beta(T_{PV} - T_{NOCT})] \quad (4)$$

describes the electrical efficiency of the PV cells, calculated considering the electrical efficiency measured at the Nominal Operating Cell Temperature (T_{NOCT}) of 323 K (η_0) and the temperature coefficient of the PV cell, β. Hence, the conversion efficiency of the incident radiation on the PV-T into electricity is assumed to decrease linearly with the operating temperature of the PV cell.

Finally, the *SSA module energy balance* considers the SSA radiative exchange with both PV cell and vessel:

$$\tau_g \int_0^\infty G(\lambda)\, \alpha_{PV}(\lambda, E_{bg})d\lambda + \varepsilon_{PV-SSA}(\lambda)\sigma(T_{PV}^4 - T_{SSA}^4) + \varepsilon_{sub-ves}\sigma(T_{ves}^4 - T_{sub}^4) = \dot{Q}_{SSA}(T_{SSA}) \quad (5)$$

where $\varepsilon_{SSA\text{-}ves}$ is the equivalent emissivity of the SSA substrate facing the underlying vessel, defined as:

Preprints (www.preprints.org) | NOT PEER-REVIEWED | Posted: 26 May 2022 doi:10.20944/preprints202205.0355.v1

$$\varepsilon_{sub-ves} = \frac{1}{\frac{1}{\varepsilon_{ves}} + \frac{1}{\varepsilon_{sub}} - 1} \quad (6)$$

and either T_{SSA} or $\dot{Q}_{SSA}(T_{SSA})$ is the third unknown of the system. In fact, $\dot{Q}_{SSA}(T_{SSA})$ represents the amount of thermal energy produced when the SSA operates at a temperature T_{SSA} lower than the stagnation temperature (T_{st}) and $\dot{Q}_{SSA}$=0 defines the stagnation condition. Hence, this set of three equations (Eqs. 1, 2, and 5) can be numerically solved either to find the equilibrium temperatures of the collector components in the stagnation conditions (when $\dot{Q}_{SSA}(T_{SSA}) = 0$) or to calculate the thermal output for a given absorber operating temperature ($T_{SSA} < T_{st}$).

2.2. Layout B: PV cell above the SSA

Design. The simplified cross-section of this layout is shown in Fig. 1 b): the PV cell is grown on the SSA. The direct contact of the PV cell with the SSA establishes a conductive exchange between the two layers; therefore, the PV cell transmittance (τ_{PV}) becomes less significant: in fact, even the heat produced by fraction of the solar spectrum below λ_{bg} that is not converted into electricity can be transferred to the SSA and collected as thermal output. Conversely, the PV cell emissivity (ε_{PV}) gains importance, as it regulates the radiative exchange towards the glass, which would result in a radiative loss. Hence, the PV cell transmittance is described as a step function with unitary and constant step height which varies with E_{bg}, while the PV cell emittance spectrum varies between 0 and 1.

Thermal model equations. As in the previous case, we consider energy balance equations for each layer.

The *glass cover energy balance* takes into account both convective losses to the external ambient and the radiative exchange with the PV cell:

$$\alpha_g \int_0^\infty G(\lambda)\, d\lambda + \hbar_w(T_{amb} - T_g) + \varepsilon_{PV-g}(\lambda, E_{bg})\sigma(T_{PV}^4 - T_g^4) = 0 \quad (7)$$

where

$$\varepsilon_{PV-g} = \frac{1}{\frac{1}{\varepsilon_{PV}} + \frac{1}{\varepsilon_g} - 1} \quad (8)$$

In the *PV module energy balance* now appears a term describing the conductive heat exchange with the SSA and a radiative loss to the glass. Also, as in the previous setup, part of the absorber radiation is converted in electrical power:

$$\tau_g \int_0^\infty G(\lambda)\, \alpha_{PV}(\lambda, E_{bg}) d\lambda + \frac{k_{PV-SSA}}{\Delta t}(T_{SSA} - T_{PV}) + \varepsilon_{PV-g}(\lambda, E_{bg})\sigma(T_g^4 - T_{PV}^4) + \eta_{el}\tau_g \int_0^\infty G(\lambda)\, \alpha_{PV}(\lambda, E_{bg}) d\lambda = 0 \quad (9)$$

Note that $k_{PV\text{-}SSA}$ is the equivalent thermal conductivity of the couple PV cell-SSA, while Δt represents the total thickness of PV cell and SSA. Because the latter is negligible (approximately 200 nm), we assumed $\Delta t \approx t_{PV} = 3$ μm.

The *SSA module energy balance* considers the heat exchanges of the SSA with vessel and PV cell, respectively radiative and conductive:

$$\tau_g \int_0^\infty G(\lambda)\, \tau_{PV}(\lambda)\alpha_{SSA} d\lambda + \frac{k_{PV-SSA}}{\Delta t}(T_{PV} - T_{SSA}) + \varepsilon_{sub-ves}\sigma(T_{ves}^4 - T_{sub}^4) = \dot{Q}_{SSA}(T_{SSA}) \quad (10)$$

Hence, as already mentioned in the previous layout, the set of three equations (Eqs. 7, 9, and 10) must be solved to find the equilibrium temperatures of the collector of the absorber (if $\dot{Q}_{SSA}(T_{SSA}) = 0$) or the produced heat ($T_{SSA} < T_{st}$).

2.3. Efficiency calculation

For each layout and various SSA operating temperature in the range of 323 K to 423 K we evaluated

Preprints (www.preprints.org) | NOT PEER-REVIEWED | Posted: 26 May 2022 doi:10.20944/preprints202205.0355.v1

- **thermal efficiency**, η_{ST}, calculated as

$$\eta_{ST} = \frac{\dot{Q}_{SSA}(T_{SSA})}{\int_0^\infty G(\lambda)\, d\lambda} \tag{11}$$

- **electrical efficiency**, η_{PV},

$$\eta_{PV} = \frac{P_{el}}{P_{in}} = \frac{\eta_{el}\tau_g \int_0^\infty G(\lambda)\alpha_{PV}(\lambda,t)\, d\lambda}{\int_0^\infty G(\lambda)\, d\lambda} \tag{12}$$

- **total efficiency** of the PV-T collector, η_{TOT},

$$\eta_{tot} = \frac{P_{el} + \dot{Q}_{SSA}(T_{SSA})}{\int_0^\infty G(\lambda) d\lambda}. \tag{13}$$

The **exergetic efficiency**, η_{Ex}, also known as the *second-law efficiency*, is considered. It is the most crucial parameter for the thermal assessment of energy systems as it gives the idea of the effectiveness of a system relative to its performance in reversible conditions. Its definition is based on the Carnot efficiency, $\eta_C = 1\text{-}T_{amb}/T_{SSA}$:

$$\eta_{Ex} = \frac{P_{el} + \dot{Q}_{SSA}(T_{SSA}) \cdot \eta_C}{(1 - \frac{T_{amb}}{T_{SUN}}) \cdot \int_0^\infty G(\lambda)\, d\lambda} \tag{14}$$

3. Results

In the following, we show the relevant results of our analysis divided in two different sub-sections, one for each layout investigated. A comparison between the two layouts has also been carried out.

3.1. Layout A: thermal and electrical efficiencies

The study conducted on layout **A** (PV cell placed under the highly transparent glass) provided a stagnation temperature for the SSA in the range of 385 K to 660 K, depending on the PV cell transmittance and bandgap energy (Fig. 2 c)). As expected, both the PV cell and the glass experience a lower temperature gradient, varying from 360 K to 410 K (Fig. 2 a) and b)). It can be noted how, for τ_{PV}= 0, the increasing of the PV cell bandgap energy E_{bg} translates into a decreasing of the PV cell temperature, due to a smaller fraction of the solar spectrum absorbed. The PV cell temperature reaches a minimum at approximately E_{bg} = 2.3 eV, whereas above this value the temperature increases again due to the thermal load originated from the high temperature of the SSA (at approximately 600 K).

The analysis conducted on the electrical and thermal efficiencies are reported in Fig. 3 a)-d) and Fig. 3 e)-h), respectively, for different SSA working temperatures. Results showed that the electrical efficiency only slightly depends on the change in the absorber temperature (Fig. 3 a)-d)). The maximum electrical efficiency curve is reminiscent of the Shockley–Queisser limit curve and scales with the cell transparency.

Preprints (www.preprints.org) | NOT PEER-REVIEWED | Posted: 26 May 2022 doi:10.20944/preprints202205.0355.v1

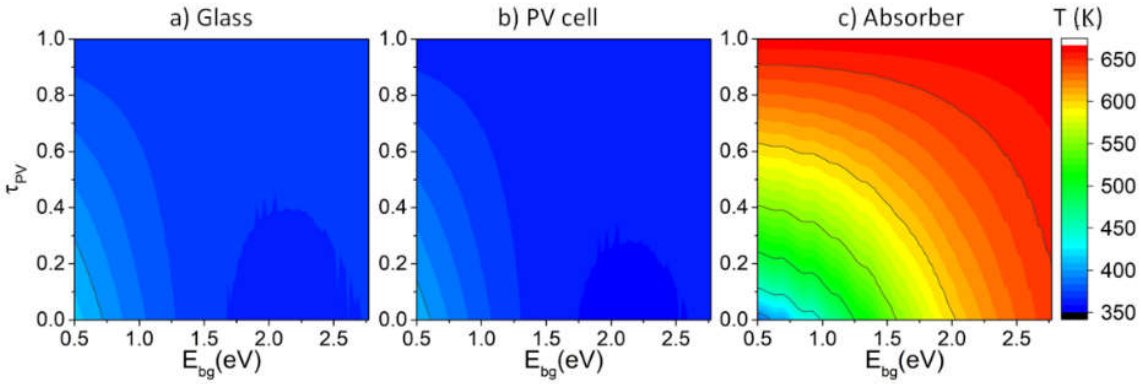

Figure 2. Glass a), PV cell b), and SSA c) temperature at the stagnation point for different values of τ_{PV} and E_{bg} (layout **A**).

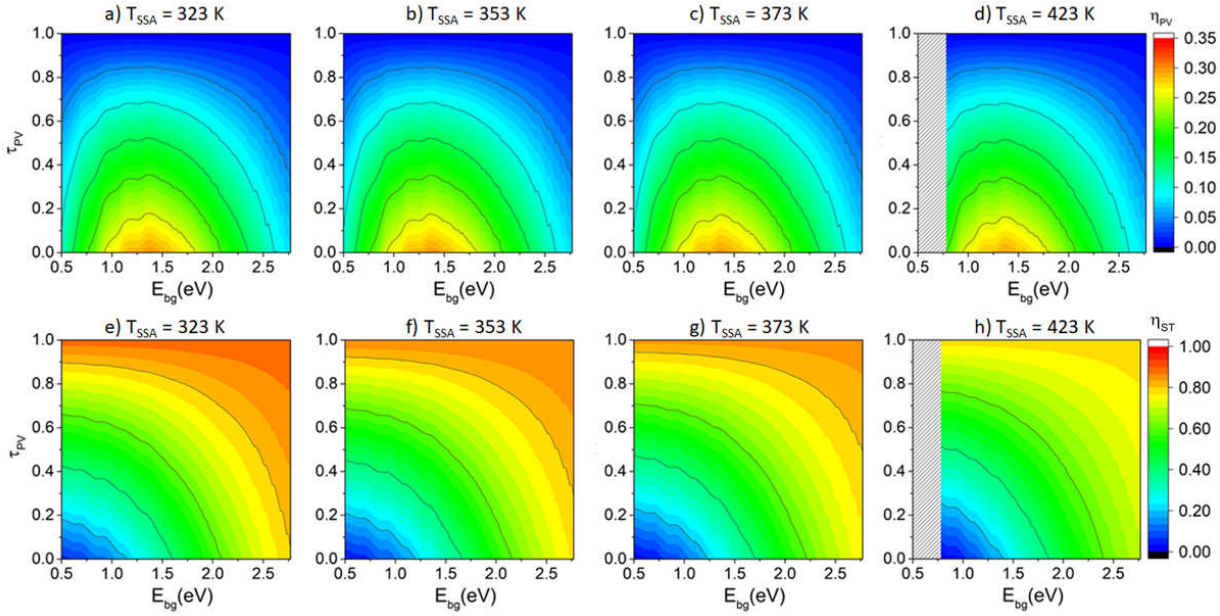

Figure 3. Electrical (a-d) and thermal (e-h) efficiency of a PV-T collector in layout **A** at different PV cell transmittance and bandgap, and at various temperatures: 323 K (a, e), 353 K (b, f), 373 K (c, g), 423 K (d, h).

At each SSA temperature, the maximum electrical efficiency of approximately ≈ 30% is reached for PV cells characterized by low PV cell transmittance ($\tau_{PV} < 0.1$) and bandgap energy E_{bg} in 0.90-1.75 eV. For E_{bg} lower than 0.8 eV the fraction of the solar spectrum transmitted to the SSA is not sufficient to bring the SSA at 423 K. Hence, for such values of temperature and E_{bg} the efficiency is schematized as a dashed area in Fig. 3 d). Conversely, the maximum thermal efficiency is obtained for high values of τ_{PV} and E_{bg} (Fig. 3 e)-h)). At a fixed PV cell bandgap energy and transmittance, the thermal power decreases with increasing the SSA working temperature. In addition, at a fixed PV cell transmittance, the thermal efficiency increases with increasing the bandgap energy, at the expense of electrical efficiency. In this setup, the PV cell temperature below T_{st} only slightly depends on T_{SSA} (Fig. 4).

Preprints (www.preprints.org) | NOT PEER-REVIEWED | Posted: 26 May 2022 doi:10.20944/preprints202205.0355.v1

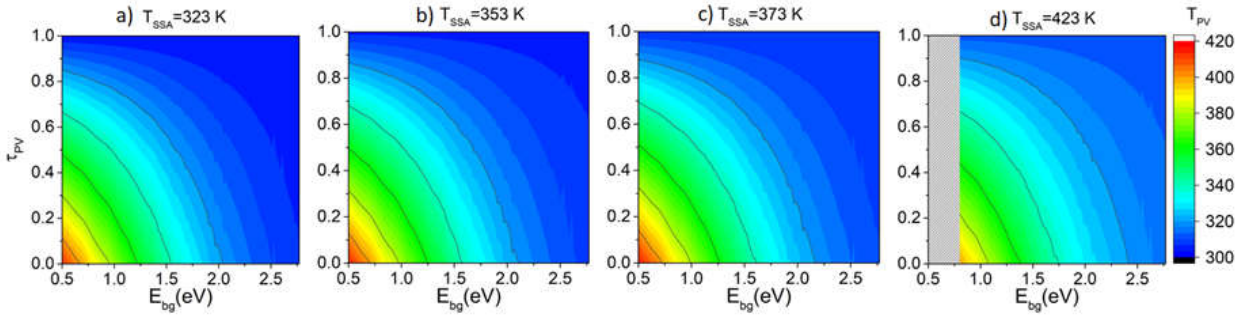

Figure 4. PV cell temperature (layout **A**) at different SSA operating temperatures: 323 K (a), 353 K (b), 373 K (c), 423 K (d). The black lines correspond to the numerical values reported in the legend on the right.

3.2. Layout B: thermal and electrical efficiencies

The study conducted on layout **B** (PV cell placed right above the SSA) showed that, at the stagnation point, the PV cell temperature is strongly dependent on that of the SSA, due to the conductive exchange between the two layers. Conversely, the glass temperature is much lower and varies by approximately 20 K in 393 - 413 K (Fig. 5). To avoid unreal stagnation temperatures, the study is limited to thermal emittances equal to or higher than 0.1. Below such value, the thermal emittance is represented by a dashed area in Fig. 5 a)-c).

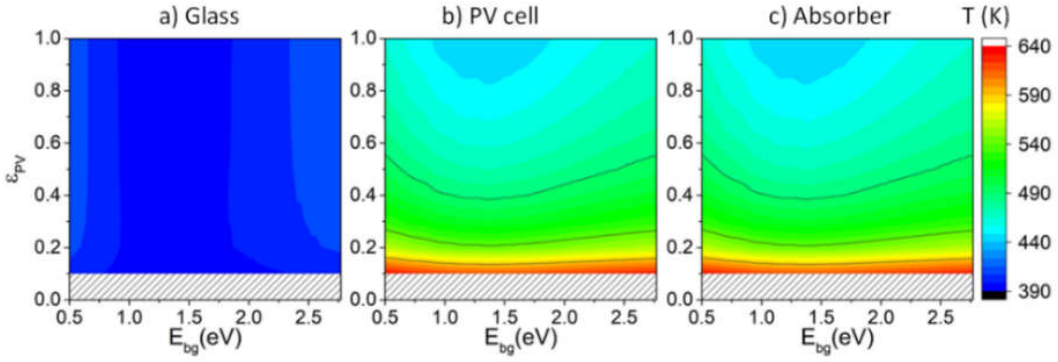

Figure 5. Glass a), PV cell b), and SSA c) temperature at the stagnation point for different values of ε_{PV} and E_{bg} (layout **B**).

At temperatures below the absorber stagnation temperature, the analysis shows that the electrical efficiency of the PV-T collector in layout **B** strongly depends on the PV cell bandgap energy, whereas its variation with the cell emissivity is negligible. At a fixed T_{SSA}, the electrical efficiency reaches its maximum (> 0.25) for E_{bg} of 1.0-1.5 eV, where the thermal counterpart experiences the maximum reduction. However, at fixed conditions, both quantities experience a decrease with the increasing of the SSA operating temperature. The results of this analysis are depicted in Fig. 6 a)-d) for the electrical efficiency and e)-h) for thermal efficiency.

In this layout, the maximum of electrical efficiency (approximately 30%) is obtained at T_{SSA}= 323 K and for bandgap energies in the range of 1 to 1.6 eV (Fig. 6 a)). As expected, results show that the temperature reached by the PV cell matches with T_{SSA} and is independent on the bandgap energy. Consequently, the electrical efficiency reduces with the operating temperature.

Preprints (www.preprints.org) | NOT PEER-REVIEWED | Posted: 26 May 2022 doi:10.20944/preprints202205.0355.v1

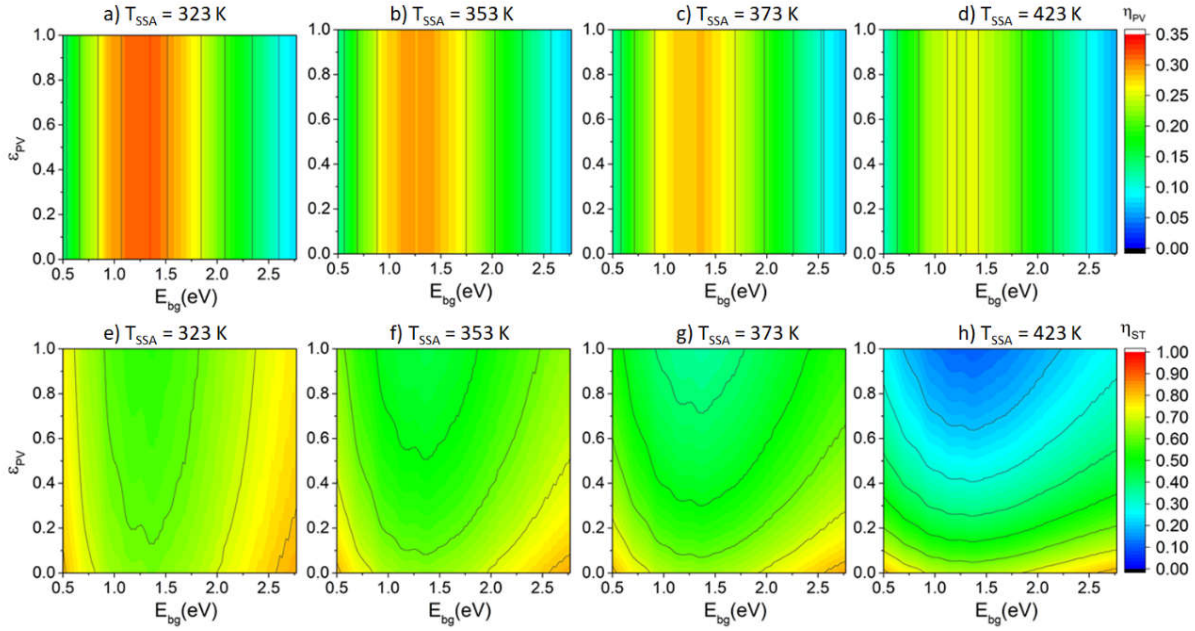

Figure 6. Electrical (a-d) and thermal (e-h) efficiency of a PV-T collector in layout **B** at different PV cell emittance and bandgap, and at various SSA operating temperatures: 323 K (a, e), 353 K (b, f), 373 K (c, g), 423 K (d, h).

3.3. Comparison between the two layouts of PV-T systems

The various efficiency contributions - e.g., thermal, electrical, total, exergetic - have been calculated for both layouts and various absorber temperatures (Fig. 7). The comparison between the two models of PV-T systems shows that the total efficiency (Eq. 13) considerably increases with the increase of E_{bg} for the collector in layout **A**, while slightly decreases when the PV cell is placed above the SSA (layout **B**). We limit the comparison between the two layouts to the most efficient cases, i.e., $\tau_{PV}(\lambda) = 0$ for layout **A** and $\varepsilon_{PV} = 0.1$ for layout **B.**

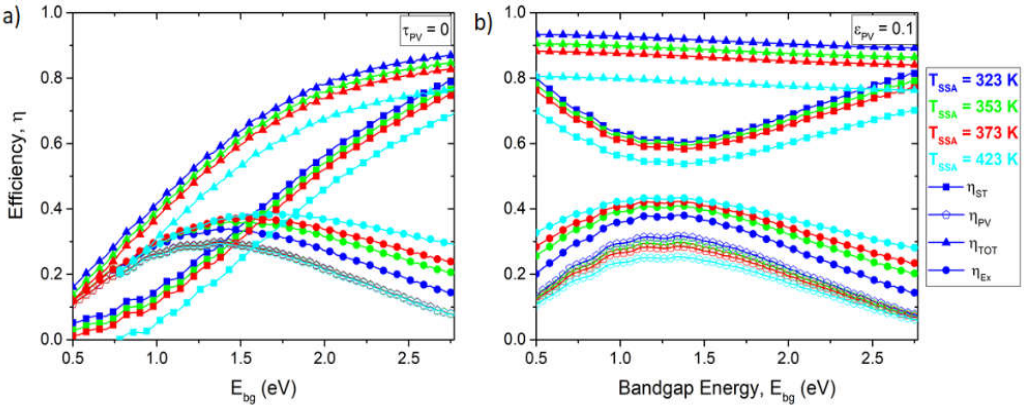

Figure 7. Thermal (η_{ST}, squares), electrical (η_{PV}, empty pentagons), total (η_{TOT}, triangles), exergetic (η_{Ex}, circles) efficiencies calculated for a) layout **A** and b) layout **B** at various absorber temperatures: 323 K (blue curves), 353 K (green curves), 373 K (red curves), and 423 K (cyan curves). Note that the PV cell transmittance and emittance have been fixed: τ_{PV}=0 for layout **A** and ε_{PV}=0.1 for layout **B**.

As for the exergetic component (Eq. 14), the model shows that both layouts allow to produce an exergy higher than that produced by a single PV cell, particularly at high T_{SSA}. For layout **A** the maximum exergy is produced at approximately E_{bg}= 1.50 eV, and it moves towards higher values of E_{bg} when the temperature increases (Fig. 7 a)). Instead, the maximum of exergy shifts towards lower energies (≈ 1.25 eV) if the cell is placed above the SSA: in this configuration the PV cell bandgap energy plays a more important role

Preprints (www.preprints.org) | NOT PEER-REVIEWED | Posted: 26 May 2022 doi:10.20944/preprints202205.0355.v1

(Fig. 7 b)). Fig. 7 shows that, particularly at high operating temperatures, moving around these E_{bg} values, the relative amount of electricity and heat produced changes, but the exergetic efficiency is not significantly affected. Both material and thickness of the PV cell can be chosen to regulate the relative amount of electrical and thermal outputs, according to the energy demand. It is also clear that electrical efficiency reduces with temperature in layout **B**, whereas it remains unchanged in layout **A**.

A deeper analysis of the exergetic efficiency has been performed by varying the PV cell transmittance/emittance values. Results are presented as colormaps in Fig. 8 a)-d) for layout **A** and Fig. 8 e)-h) for layout **B**. The latter study highlights the importance of controlling the value of ε_{PV} to obtain a high η_{Ex}, particularly at high T_{SSA} (Fig. 8 g)-h)).

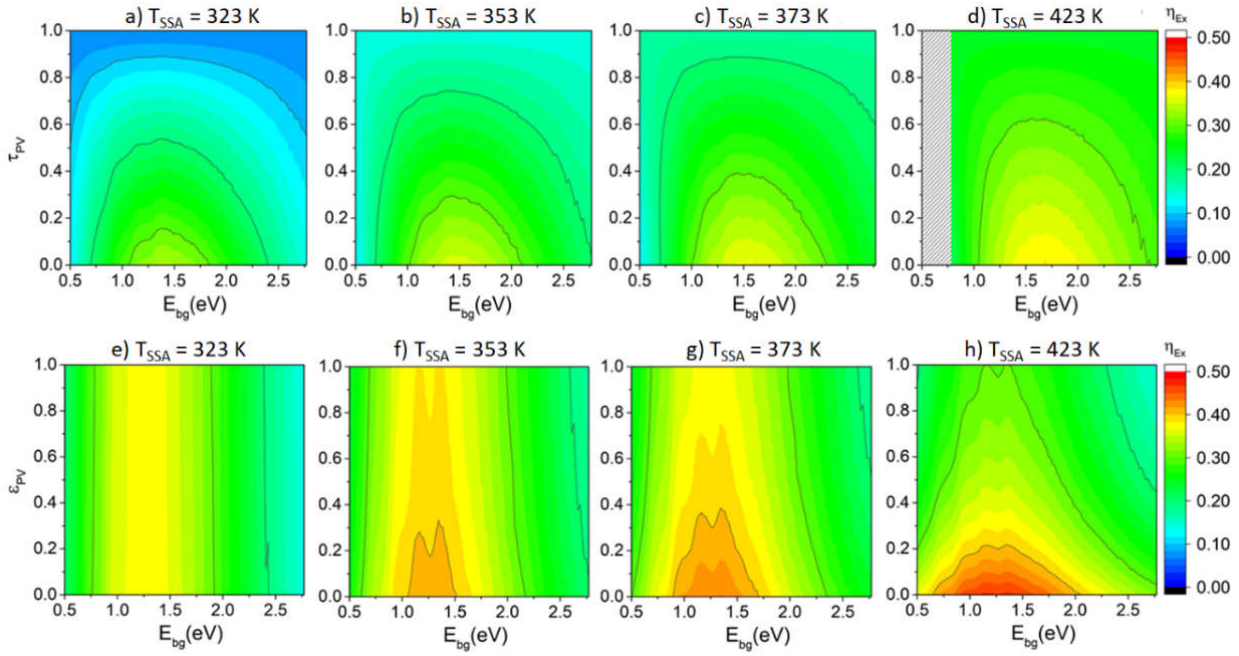

Figure 8. Exergetic efficiency of a PV-T collector in layout **A** (a)-d)) and **B** (e)-h)) at different PV cell emittance and bandgap and various SSA operating temperatures: 323 K (a, e), 353 K (b, f), 373 K (c, g), 423 K (d, h).

4. Conclusion

In this work the investigation of the performance of two layouts of novel flat photovoltaic-thermal (PV-T) modules under vacuum is carried out through a 1D (dimensional) steady-state-energy-balance numerical model. The PV cell can be either placed below the glass encapsulating the solar collector (layout **A**) or in a direct contact with the absorber (layout **B**). The thermal, electrical, total (thermal+electrical), and exergetic efficiencies have been estimated, assuming a variable transmittance or emittance of the PV cell, depending on the layout.

The analysis shows that, if on the one hand the PV cell is placed under the glass (layout **A**), the PV-T system can efficiently produce electrical and thermal energy. Using high bandgap materials, it is possible to obtain a PV cell temperature close to ambient temperature, and let a larger fraction of the solar spectrum reach the SSA to produce thermal heat at temperatures as high as 150 °C. If, on the other hand, the photovoltaic cell is placed above the absorber (layout **B**), the maximum of electrical efficiency can be obtained at T_{SSA} = 323 K and for PV cell with bandgap energy in the range of 1.1 eV to 1.5 eV. Increasing the operating temperature, it became essential to obtain low emittance values to reach high thermal and exergy efficiencies.

Overall, the work highlights the importance of the high vacuum insulation, which reduces convective and conductive losses to negligible levels, and indicates that it is possible to fully exploit the solar spectral radiation and maximize the generation of usable

 doi:10.20944/preprints202205.0355.v1

energy (electrical and heat) by rethinking the solar energy conversion process from the point of view of the energy demand. The energy and exergy efficiencies obtainable from the proposed PV-T systems are considerably improved compared to results of the previous literature: with such a promising prospect, PV-Ts can certainly be part of future highly efficient and climate neutral multi-energy systems that hold the key for an accelerated and full decarbonization of the global economy.

Acknowledgments: The Ph.D. grant of A.C is funded by the PON2014-2020 "Dottorati innovativi con caratterizzazione industriale" program XXXV and XXXIV ciclo. The Ph.D. grant of E.G is funded by the CNR-Confindustria "Dottorati di Ricerca Industriali" program XXXVI ciclo.

Nomenclature

Abbreviations and subscripts

abs	Absorber
amb	Ambient
bg	Bandgap
C	Carnot
E	Energy, eV
Ex	Exergy
I	Solar irradiance, W m^{-2}
g	Glass
k	Thermal conductivity, W m^{-1} K^{-2}
NOCT	Nominal Operating Cell Temperature
PV	Photovoltaic
PV-T	Photovoltaic-Thermal
SSA	Selective Solar Absorber
ST	Solar Thermal
t	Thickness, m
T	Temperature, K
st	Stagnation
sub	Substrate
tot	Total
ves	Vessel
w	Wind

Greek Symbols

α	Absorptance
β	Temperature coefficient, % K^{-1}
η	Efficiency
λ	Wavelength, μm
σ	Stefan-Boltzmann constant, W m^{-2} K^{-4}
τ	Transmittance
ε	Emissivity

References

[1] M. A. Green, E. D. Dunlop, J. Hohl-Ebinger, M. Yoshita, N. Kopidakis, and A. W. Y. Ho-Baillie. (2020) "Solar cell efficiency tables (Version 55)." *Prog. Photovolt. Res. Appl.* 28.1 (2020): 3–15.

[2] H. G. Teo, P. S. Lee, and M. N. A. Hawlader. (2012) "An active cooling system for photovoltaic modules." *Appl. Energy* 90.1 (2012): 309-315.

[3] S. Dubey, J. N. Sarvaiya, and B. Seshadri. (2013) "Temperature Dependent Photovoltaic (PV) Efficiency and Its Effect on PV Production in the World – A Review." *Energy Procedia* 33 (2013):311–321.

[4] M. Herrando, C. N. Markides, and K. Hellgardt. (2014) "A UK-based assessment of hybrid PV and solar-thermal systems for domestic heating and power: System performance." *Appl. Energy* 122 (2014): 288–309.

[5] C. de Keizer *et al.* (2016) "Evaluating the Thermal and Electrical Performance of Several Uncovered PVT Collectors with a Field Test." *Energy Procedia* 91 (2016): 20–26.

[6] T. T. Chow. (2010) "A review on photovoltaic/thermal hybrid solar technology." *Appl. Energy* 87. 2 (2010): 365–379

 doi:10.20944/preprints202205.0355.v1

[7] H. Zondag. (2008) "Flat-plate PV-Thermal collectors and systems: A review." *Renew. Sustain. Energy Rev.* 12.4 (2008): 891–959.
[8] S. S. S. Baljit *et al.* (2017) "Mathematical modelling of a dual-fluid concentrating photovoltaic-thermal (PV-T) solar collector." *Renew. Energy* 114 (2017):1258–1271
[9] A. K. Khlief, S. I. Ul Haq Gilani, H. H. Al-Kayiem, and S. T. Mohammad. (2021) "Concentrated solar tower hybrid evacuated tube photovoltaic/thermal receiver with a non-imaging optic reflector: A case study." *J. Clean. Prod.* 298 (2021):126683.
[10] K. Sahlaoui, H. Oueslati, and S. B. Mabrouk. (2021) "Thermal and electrical performance evaluation of hybrid air PV/T collector –numerical analysis and experimental study." *Int. J. Sustain. Energy* 40. 9 (2021):889–909.
[11] T. Salameh, M. Tawalbeh, A. Juaidi, R. Abdallah, and A.-K. Hamid. (2020) "A novel three-dimensional numerical model for PV/T water system in hot climate region." *Renew. Energy* 164 (2021): 1320–1333.
[12] Y. Maleki, F. Pourfayaz, and M. Mehrpooya. (2021) "Transient optimization of annual performance of a photovoltaic thermal system based on accurate estimation of coolant water temperature: A comparison with conventional methods." *Case Stud. Therm. Eng.* 28 (2021):101395.
[13] M. Herrando, R. Simón, I. Guedea, and N. Fueyo. (2020)"The challenges of solar hybrid PVT systems in the food processing industry." *Appl. Therm. Eng.* 184 (2020):116235.
[14] S. Shaari, A. M. Omar, and M. Z. Hussin. (2014) "Simplified modeling techniques for predicting outputs of grid-connected photovoltaic power systems." *Int. J. Renew. Energy* 9.1 (2014).
[15] A. Buonomano et al. (2016) "Experimental analysis and dynamic simulation of a novel high-temperature solar cooling system," *Energy Convers. Manag.* 109 (2016): 19–39.
[16] A. Mellor *et al.* (2018) "Roadmap for the next-generation of hybrid photovoltaic-thermal solar energy collectors." *Sol. Energy* 174 (2018):386
[17] H. J. Queisser. (2009) "Detailed balance limit for solar cell efficiency." *Mater. Sci. Eng. B* 159–160 (2009): 322–328.
[18] S. Rühle. (2016) "Tabulated values of the Shockley–Queisser limit for single junction solar cells." *Sol. Energy* 130 (2016):139–147.
[19] G. Huang and C. N. Markides. (2021) "Spectral-splitting hybrid PV-thermal (PV-T) solar collectors employing semi-transparent solar cells as optical filters." *Energy Convers. Manag.* 248 (2021):114776.
[20] "TVP Solar." https://www.tvpsolar.com/
[21] C. D'Alessandro *et al.* (2021) "Performance analysis of evacuated solar thermal panels with an infrared mirror." *Appl. Energy* 288 (2021):116603.
[22] D. De Maio *et al.* (2021) "A Selective Solar Absorber for Unconcentrated Solar Thermal Panels." *Energies* 14.4 (2021): 900.
[23] D. De Maio *et al.* (2021) "Multilayers for efficient thermal energy conversion in high vacuum flat solar thermal panels." *Thin Solid Films* 735 (2021):138869
[24] "Infinity PV." https://infinitypv.com/learn/virtual-tools/b01
[25] T. Sample and A. Virtuani. (2009) "Modification to the Standard Reference Environment (SRE) for Nominal Operating Cell Temperature (NOCT) to Account for Building Integration." *24th Eur. Photovolt. Sol. Energy Conf.* 21-25 September 2009.